Check for updates

Gaining insight into molecular tunnel junctions with a pocket calculator without *I–V* data fitting. Five-thirds protocol†

Ioan Bâldea (ID)

The protocol put forward in the present paper is an attempt to meet the experimentalists' legitimate desire of reliably and easily extracting microscopic parameters from current–voltage measurements on molecular junctions. It applies to junctions wherein charge transport dominated by a single level (molecular orbital, MO) occurs *via* off-resonant tunneling. The recipe is simple. The measured current–voltage curve $I = I(V)$ should be recast as a curve of $V^{5/3}/I$ *versus* V. This curve exhibits two maxima: one at positive bias ($V = V_{p+}$), another at negative bias ($V = V_{p-}$). The values $V_{p+} > 0$ and $V_{p-} < 0$ at the two peaks of the curve for $V^{5/3}/I$ at positive and negative bias and the corresponding values $I_{p+} = I(V_{p+}) > 0$ and $I_{p-} = I(V_{p-}) < 0$ of the current is all information needed as input. The arithmetic average of V_{p+} and $|V_{p-}|$ in volt provides the value in electronvolt of the MO energy offset $\varepsilon_0 = E_{MO} - E_F$ relative to the electrode Fermi level ($|\varepsilon_0| = e(V_{p+} + |V_{p-}|)/2$). The value of the (Stark) strength of the bias-driven MO shift is obtained as $\gamma = (4/5)(V_{p+} - |V_{p-}|)/(V_{p+} + |V_{p-}|)$ sign (ε_0). Even the low-bias conductance estimate, $G = (3/8)(I_{p+}/V_{p+} + I_{p-}/V_{p-})$, can be a preferable alternative to that deduced from fitting the *I–V* slope in situations of noisy curves at low bias. To demonstrate the reliability and the generality of this "five-thirds" protocol, I illustrate its wide applicability for molecular tunnel junctions fabricated using metallic and nonmetallic electrodes, molecular species possessing localized σ and delocalized π electrons, and various techniques (mechanically controlled break junctions, STM break junctions, conducting probe AFM junctions, and large area junctions).

1 Introduction

Conventional semiconductor microelectronics has at its disposal a series of simplified equations to easily gain insight into underlying physics.[1,2] This is the case, *e.g.*, of the familiar Shockley equation ("ideal diode law"),[3–6] expressing analytically the exponential dependence of the current I on bias V stemming from the microscopically built-in potential barrier at a p–n junction.

In an attempt to establish the molecular structure–tunneling transport relationship, starting from ideas put forward by Newns and Schmickler in conjunction with electro/chemisorption,[7–9] I have deduced, as a counterpart for molecular electronics, an appealingly simple formula for molecular junctions wherein thermal effects are ignored[10,11] and the off-resonant tunneling current is dominated by a single level (molecular orbital MO).[12]

This off-resonant single level model (orSLM) expresses the current as a function of bias in terms of three key electronic

structure parameters: the MO energy offset relative to electrodes' Fermi energy $\varepsilon_0 = E_{MO} - E_F$, the average MO coupling $\Gamma = \sqrt{\Gamma_s \Gamma_t}$ to the two (generic substrate s and tip t) electrodes, and the bias-driven MO shift γ

$$I \equiv I(V; \varepsilon_0, \gamma, G) = \frac{G\varepsilon_0^2 V}{\varepsilon_V^2 - (eV/2)^2};$$

$$\varepsilon_V = \varepsilon_0 + \gamma eV; \quad G = NG_0 \frac{\Gamma^2}{\varepsilon_0^2} \tag{1}$$

Above, $G_0 = 2e^2/h = 77.48$ μS is the conductance quantum and N is the number of molecules per junction. Within eqn (1), asymmetric *I–V* curves (current rectification) correspond to junctions where the MO energy is shifted by an applied bias ($\gamma \neq 0$). *I–V* curves are symmetric (no current rectification) in the absence of a bias-driven MO shift ($\gamma = 0$, $\varepsilon_V = \varepsilon_0$). To be sure, aiming at describing charge transport by tunneling in situations where thermal effects are negligible, eqn (1) has limits of validity precisely formulated.[10,11] They should strictly be observed in specific applications to real molecular junctions.

Methodological advantages of the orSLM approach have been highlighted recently.[13] One particular aspect worth mentioning is the excellent agreement between the MO offset

Theoretical Chemistry, Heidelberg University, Im Neuenheimer Feld 229, D-69120 Heidelberg, Germany. E-mail: ioan.baldea@pci.uni-heidelberg.de; Fax: +49 6221 545221; Tel: +49 6221 545219

† Electronic supplementary information (ESI) available: Additional details and figures. See DOI: https://doi.org/10.1039/d4cp00217b

This journal is © the Owner Societies 2024

extracted from transport data and the MO offset obtained from a completely different method, namely independent ultraviolet photoelectron spectroscopy (UPS) data. This finding is all the more important, since it has been reported for completely different homologous molecular series.[14–16] This agreement represents perhaps the strongest support that validates the analysis based on the orSLM.

Fitting measured I–V data to eqn (1) and extracting best fitting parameters ε_0, Γ (or the low bias conductance G, to which I will loosely refer as a "microscopic" parameter in order to obviate lengthy discussions for junctions with $N > 1$), and γ should pose no special problem. This is confirmed by numerous applications of the orSLM approach by many independent groups,[17–41] which succeeded in correctly reproducing I–V curves measured for molecular junctions fabricated using various techniques.

Notwithstanding the aforementioned, publications also exist wherein, unfortunately, model parameter values have been incorrectly determined data fitting to eqn (1). Because emphasis in this paper is on how to easily and correctly estimate microscopic parameters by means of the orSLM, I intentionally refrain from citing misapplications of this approach. Still, I want to mention a frequent error that can be immediately identified. Those publications report MO offsets $|\varepsilon_0|(<eV/2)$ incompatible with the bias range $(-V, +V)$ used for data fitting. This can be easily seen by inspecting eqn (1), wherein the denominator becomes negative at too higher biases, beyond the scope of this model. This corresponds to a completely nonphysical situation wherein the current and bias have opposite signs. In fact, as reiterated again and again,[10,11] a

necessary ("off-resonance") condition for eqn (1) to apply is that of sufficiently lower biases (usually $e|V| \lesssim 1.4|\varepsilon_0|$).

Below, I will show that and how the microscopic parameters ε_0, γ and G can be directly estimated from appropriately recasting the measured I–V curves obviating the usage of eqn (1) with adjustable model parameters which could lead to the unpleasant situations referred to in the preceding paragraph.

Before proceeding, let me emphasize what is already expressed by the title of this paper. My present aim is to demonstrated that, provided that conditions of validity clearly stated are fulfilled (see ref. 10 and 42 and Fig. 1 below), the orSLM allows to estimate microscopic parameters characterizing real molecular tunnel junctions obviating I–V data fitting. For this reason, a comparison with other data fitting approaches from the literature[43–49] would be misplaced and will not be attempted.

2 Basic working equations

Aiming at providing a theoretical basis and generalizing the transition voltage spectroscopy (TVS) approach proposed by Frisbie et al.,[50] I showed that the parameters ε_0 and γ can be estimated from the so-called transition voltages $V_{t\pm}$[12]

$$|\varepsilon_0| = 2\frac{eV_{t+}|V_{t-}|}{\sqrt{V_{t+}{}^2 + 10V_{\kappa+}|V_{\kappa-}|/3 + V_{\kappa-}{}^2}} \quad (2a)$$

$$\gamma = \frac{\text{sign}\varepsilon_0}{2}\frac{V_{t+} - |V_{t-}|}{\sqrt{V_{t+}{}^2 + 10V_{t+}|V_{t-}|/3 + V_{t-}{}^2}} \quad (2b)$$
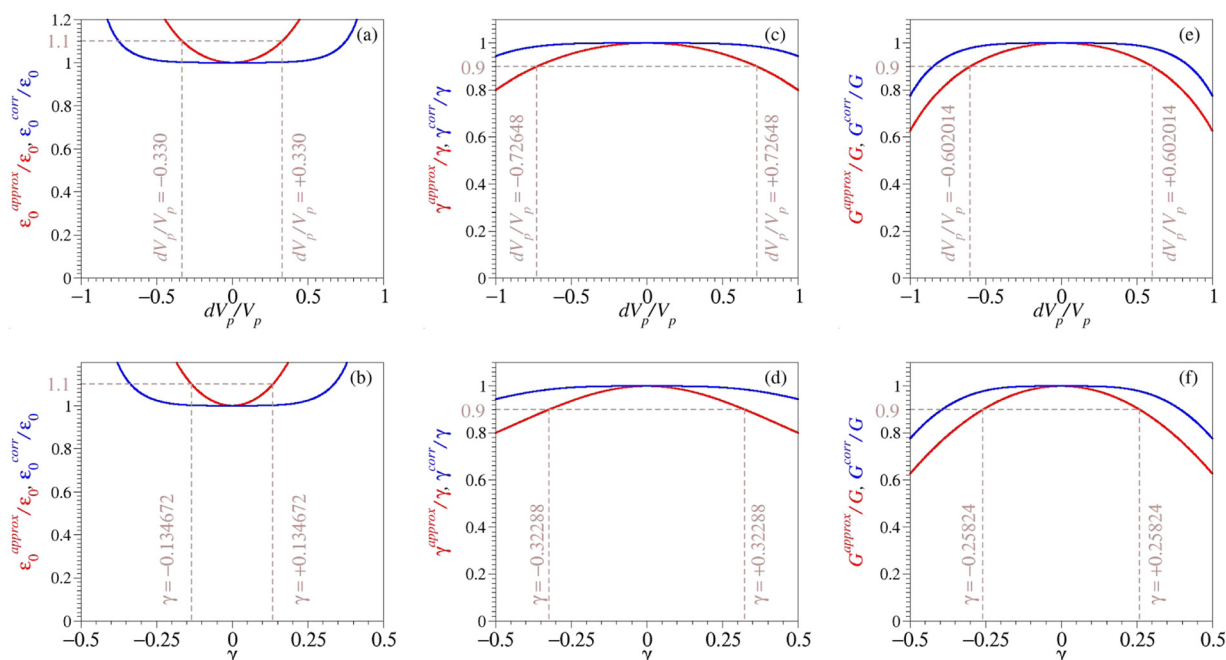

Fig. 1 Relative deviations from the exact values of the model parameters ε_0, γ, and G computed by eqn (9) and (10) (red and blue lines, respectively) plotted *versus* the relative peak asymmetry location $\delta V_p/V_p$ (left panels a, c, e) and *versus* the bias-driven MO shift γ (right panels b, d, f). The vertical brown lines visualize the ranges within which the parameters estimated *via* eqn (9) are accurate within 10%, a typical value for experimental inaccuracies in real molecular junctions.

This journal is © the Owner Societies 2024

Phys. Chem. Chem. Phys., 2024, **26**, 8724–8733 | **8725**

$V_{t+}(>0)$ and $V_{t-}(<0)$ can be defined as the positive and negative values of the bias where $\ln|I/V^2|$ is minimum[50] or $V^2/|I|$ is maximum,[51,52] or, mathematically equivalently, where the differential conductance is two times larger than the nominal (pseudo-ohmic) conductance[53]

$$\left.\frac{V^2}{|I|}\right|_{V=V_t} = \max \Leftrightarrow \left.\frac{\partial I}{\partial V}\right|_{V=V_t} = 2\left.\frac{I}{V}\right|_{V=V_t} \quad (3)$$

Eqn (3) can be easily deduced:[12] one should plug the expression for the current (eqn (1) into eqn (3)) and solve the ensuing quadratic equation.

Eqn (3) is a particular case ($\kappa = 2$) of a more general condition

$$\left.\frac{|V|^\kappa}{|I|}\right|_{V=V_\kappa} = \max \Leftrightarrow \left.\frac{\partial I}{\partial V}\right|_{V=V_\kappa} = \kappa\left.\frac{I}{V}\right|_{V=V_\kappa} \quad (4)$$

for which the counterpart of the particular eqn (2) can also be deduced analytically[12]

$$|\varepsilon_0| = \frac{\kappa(\kappa+1)}{\kappa^2-1}\frac{eV_{\kappa+}|V_{\kappa-}|}{\sqrt{V_{\kappa+}^2+2\frac{\kappa^2+1}{\kappa^2-1}V_{\kappa+}|V_{\kappa-}|+V_{\kappa-}^2}} \quad (5a)$$

$$\gamma = \frac{\mathrm{sign}\varepsilon_0}{2}\frac{V_{\kappa+}-|V_{\kappa-}|}{\sqrt{V_{\kappa+}^2+2\frac{\kappa^2+1}{\kappa^2-1}V_{\kappa+}|V_{\kappa-}|+V_{\kappa-}^2}} \quad (5b)$$

Above, $V_{\kappa+}$ and $V_{\kappa-}$ are the positive and negative biases at the peaks of the plot of $|V|^\kappa/|I|$ *versus* V. Eqn (5) can also be easily deduced:[12] one should plug the expression for the current (eqn (1) into eqn (4)) and solve the quadratic equation thus obtained.

As will be seen shortly below, the formulas for $\kappa = 5/3$ are particularly interesting

$$|\varepsilon_0| = \frac{5}{2}\frac{eV_{p+}|V_{p-}|}{\sqrt{V_{p+}^2+\frac{17}{4}V_{p+}|V_{p-}|+V_{p-}^2}} \quad (6a)$$

$$\gamma = \frac{\mathrm{sign}\varepsilon_0}{2}\frac{V_{p+}-|V_{p-}|}{\sqrt{V_{p+}^2+\frac{17}{4}V_{p+}|V_{p-}|+V_{p-}^2}} \quad (6b)$$

In view of the special role played by the value $\kappa = 5/3$ anticipated above, I will write $V_{p\pm}$ instead of $V_{5/3\pm}$ to specify the location of the peaks of $|V|^{5/3}/|I|$

$$\frac{|V|^{5/3}}{|I|} = \max \Leftrightarrow V = V_{p\pm}(\equiv V_{5/3,\pm}) \quad (6c)$$

In principle, the parameters ε_0 and γ can be computed from $V_{p\pm}$ *via* eqn (6) just as these parameters can be calculated from the transition voltages $V_{t\pm}$ *via* eqn (2) (or, in general, from $V_{\kappa\pm}$ *via* eqn (5)).

The reason why $\kappa = 5/3$ is a special value becomes clear by considering the case of symmetric I–V curves ($\gamma = 0$, *cf.* eqn (1)). In such cases the peaks of $V^{5/3}/I$ are located symmetrically around origin ($V_{5/3+} = |V_{5/3-}| \equiv V_p$) and eqn (6a) reduces to

$$\gamma = 0 \rightarrow |\varepsilon_0| = eV_p \quad (7)$$

That is, eqn (7) allows the most straightforward determination of the MO energy offset from the current–voltage measurements. What one has to do in order to estimate the MO offset ε_0 of a junction with symmetric I–V characteristic is merely to draw a plot of $V^{5/3}/I$ *versus* V. Expressed in electronvolt, the value of the MO energy offset (ε_0) is equal to the magnitude in volt of the bias ($V_p = V_{p+} = |V_{p-}|$) at which the two symmetric peaks of the curve for $V^{5/3}/I$ are located.

To be sure, eqn (7) applies to molecular junctions having symmetric I–V characteristics ($I(-V) = -I(V)$) while real junctions often possess asymmetric characteristics ($I(-V) \neq -I(V)$). Within the orSLM this asymmetry (current rectification) stems from a nonvanishing value $\gamma \neq 0$ (*cf.* eqn (1)).

Because a nonvanishing γ is directly related (*cf.* eqn (6b)) to an asymmetric location of the peaks of $V^{5/3}/I$ around origin ($V_{p+} \neq -V_{p-}$), it makes sense to define an average peak voltage V_p and to consider Taylor series expansions of eqn (6) in terms of the departure δV_p of $V_{p\pm}$ from the average V_p

$$V_p \equiv \frac{V_{p+}+|V_{p-}|}{2} = \frac{V_{p+}-V_{p-}}{2}(>0) \quad (8a)$$

$$V_{p\pm} = \pm V_p + \delta V_p; \ \delta V_p = \frac{V_{p+}-|V_{p-}|}{2}\left(\begin{smallmatrix}\leq\\>\end{smallmatrix}0\right) \quad (8b)$$

The lowest order expansion of eqn (6) (*i.e.*, neglecting all powers of δV_p in the Taylor series) yields the following approximate expressions

$$|\varepsilon_0| \approx |\varepsilon_0^{\mathrm{approx}}| = eV_p = e\frac{V_{p+}+|V_{p-}|}{2} \quad (9a)$$

$$\gamma \approx \gamma^{\mathrm{approx}} = \frac{2}{5}\frac{\delta V_p}{V_p}\mathrm{sign}\varepsilon_0 = \frac{4}{5}\frac{V_{p+}-|V_{p-}|}{V_{p+}+|V_{p-}|}\mathrm{sign}\varepsilon_0 \quad (9b)$$

$$G \approx G^{\mathrm{approx}} = \frac{3}{8}\left(\frac{I_{p+}}{V_{p+}}+\frac{I_{p-}}{V_{p-}}\right); \ I_{p\pm} \equiv I(V_{p\pm}) \quad (9c)$$

Eqn (9) shows that all three parameters ε_0, γ, and G that microscopically characterize a tunneling junction can be estimated from four experimental quantities only, which can directly extracted from I–V measurements: the positive and negative bias $V_{p\pm}$ where the peaks of the curve $|V|^{5/3}/|I|$ are located and the corresponding currents $I_{p\pm}$.

Notice that in addition to ε_0, γ, eqn (9c) presents an approximate estimate for the low bias conductance G. It has been deduced by series expansion of G expressed using eqn (1). Although G is routinely determined by linear fitting of low V data, the estimate *via* eqn (9c) may be preferable in cases of noisy data at low bias. This may be a relevant aspect for reliably determining the tunneling attenuation β from conductances $G_n \propto \exp(-\beta n)$ of menbers of variable size n of a homologous series.

3 Accuracy of the lowest order approximation

The smaller the asymmetry δV_p (or, alternatively, the smaller the value or γ), the better the lowest order approximation

8726 | *Phys. Chem. Chem. Phys.*, 2024, **26**, 8724–8733

This journal is © the Owner Societies 2024

underlying eqn (9), but the question relevant for practice is how good this approximation actually is.

To illustrate the accuracy of the lowest order approximation, in Fig. 1 I depicted by red lines departures from the exact values of the parameters ε_0, γ, and G estimated eqn (9) both as a function of the fractional peak voltage asymmetry $\delta V_p / V_p$ (panels a, c, and e) and as a function of the bias driven MO shift (panels b, d, and f). For the reader's convenience, in Fig. 1 I drew vertical lines to delimit the range where the model parameters estimated from eqn (9) are accurate to within 10%, a value typical for accuracy in molecular electronics.

Inspection of Fig. 1 reveals that all three parameters achieve this accuracy for $|\gamma| \lesssim 0.134$. On this basis one can conclude that eqn (9) is indeed a good approximation. In saying this, I have in mind that for most real molecular tunnel junctions typical values of γ are relatively small (say $|\gamma| \lesssim 0.1$[14,15,54−56]). This is the case even for molecular junctions exhibiting substantial current rectification.[57]

To better understand why the lowest order approximations of eqn (9) are adequate for most practical purposes I present below the next-to-leading corrections (*i.e.*, retaining the terms proportional to $(\delta V_p / V_p{}^2)$ in the Taylor series)

$$\varepsilon_0 = \varepsilon_0^{\text{approx}} \underbrace{\left[1 - \frac{41}{50}\left(\frac{\delta V_p}{V_p}\right)^2\right]}_{\varepsilon_0^{\text{corr}}} + \mathcal{O}\left(\frac{\delta V_p}{V_p}\right)^4 \quad (10a)$$

$$\gamma = \gamma^{\text{approx}} \underbrace{\left[1 + \frac{9}{50}\left(\frac{\delta V_p}{V_p}\right)^2\right]}_{\gamma^{\text{corr}}} + \mathcal{O}\left(\frac{\delta V_p}{V_p}\right)^4 \quad (10b)$$

$$G = G^{\text{approx}} \underbrace{\left[1 + \frac{6}{25}\left(\frac{\delta V_p}{V_p}\right)^2\right]}_{G^{\text{corr}}} + \mathcal{O}\left(\frac{\delta V_p}{V_p}\right)^4 \quad (10c)$$

They are depicted by blue lines in Fig. 1. As visible above, terms linear in $\delta V_p / V_p$ vanish; only quadratic terms $(\delta V_p / V_p)^2$ contribute.

To avoid misuses, I want to explicitly emphasize what Fig. 1 clearly visualizes. While the general orSLM model can be used to quantitatively analyze molecular junctions exhibiting strong current rectification,[58,59] the five-thirds protocol cannot; it is designed to deal expeditiously with cases wherein current rectification is not very pronounced.

4 Practical recipe for the application of the five-thirds protocol

Fig. 2 illustrates how to apply the presently proposed five-thirds protocol to estimate the parameters for molecular junctions possessing symmetric and asymmetric *I–V* characteristics (additional details in the ESI†):

(i) Recast the measured *I–V* data (panels a and c) as a plot of $|V|^{5/3}/|I|$ *versus* V (panels b and d).
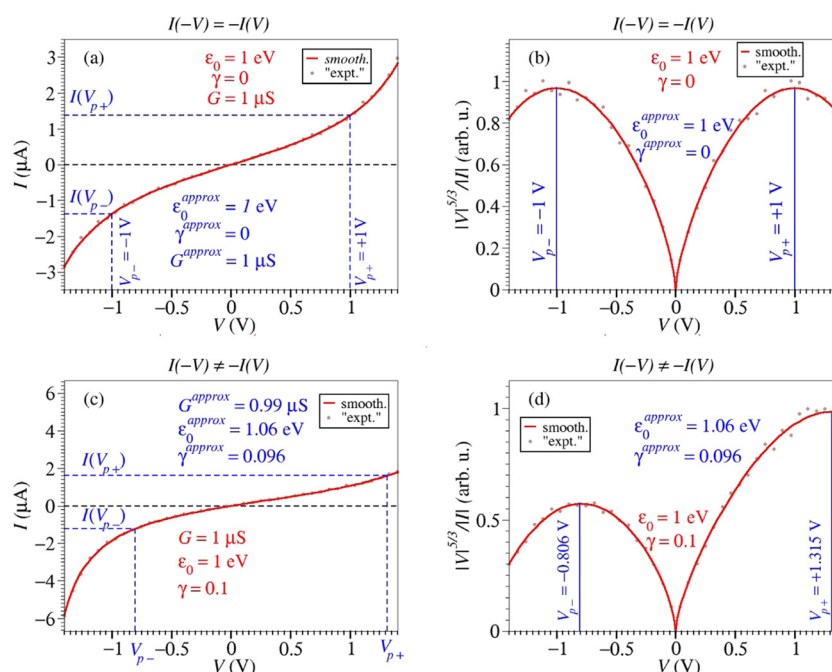

Fig. 2 Schematic illustration of the five-thirds protocol at work for junctions with symmetric *I−V* characteristics (panels a and b) and asymmetric *I−V* characteristics (panels c and d). The red curves computed by using eqn (1) and parameter values depicted in red which mimic real *I−V* curves of panel a and c are recast as plots of $|V|^{5/3}/|I|$ *versus* bias (V) in panel b and d. The maximum locations at $V_{p\pm}$ extracted from the right panels along with the corresponding current values $I_{p\pm}$ obtained from the left panels are used to estimate the model parameters ε_0, γ, and G via eqn (9). The weak disorder (brown points) overimposed on the red *I−V* curves is intended to give a flavor of how applications to real junctions look like.

This journal is © the Owner Societies 2024

Phys. Chem. Chem. Phys., 2024, **26**, 8724–8733 | **8727**

(ii) Extract the values of the peak voltages V_{p+} and V_{p-} from the maxima of $|V|^{5/3}/|I|$ at positive and negative bias. These values allow the straightforward determination of the MO energy offset ε_0 and the MO bias-driven shift γ via eqn (9a) and (9b), respectively. In cases of symmetric I–V curves $V_{p+} = -V_{p-} = V_p$ ($\gamma = 0$) and $|\varepsilon_0| = eV_p$. To accurately extract the peak positions ($V_{p\pm}$), noisy curves should be smoothed beforehand. This is a straightforward task for common software utilized by experimentalists (*e.g.*, ORIGIN).

(iii) With the values of V_{p+} and V_{p-} in hand, return to the I–V curves and extract the values of the current I_{p+} and I_{p-} at the biases V_{p+} and V_{p-} (Fig. 2a and c). Use these four values ($V_{p\pm}$ and $I_{p\pm}$) to estimate the low bias conductance from eqn (9c). In cases of symmetric I–V curves, $\gamma = 0$, $I_{p+} = -I_{p-} = I_p$, $V_{p+} = -V_{p-} = V_p = |\varepsilon_0|$, and eqn (9c) reduces to

$$G = \frac{3}{4}\frac{I_p}{V_p} \tag{11}$$

(iv) Inspection of Fig. 1a, c, and e allows one to assess the accuracy/reliability of the parameters ε_0, γ, and G estimated via eqn (9) at the value of $\delta V_p/V_p$ computed from the values V_{p+} and V_{p-} directly extracted from the experimental I–V data in question without any assumption.

5 Applications to real junctions

To emphasize the generality of the presently proposed five-thirds protocol, I will consider junctions fabricated with the most frequently utilized fabrication platforms: single-molecule mechanically-controlled break junctions, single-molecule STM break junctions ($N = 1$), CP-AFM molecular junctions ($N \sim 100$), and large area molecular junctions ($N \gg 1$).

As noted on several occasions (*e.g.*, ref. 11) I–V data alone do not suffice to specify whether conduction is of p-type ($\varepsilon_0 < 0$) or n-type ($\varepsilon_0 > 0$) (*i.e.*, mediated by an occupied or an unoccupied MO, respectively). However, in order to simplify the analysis of the real junctions considered below, I will (arbitrarily) "postulate" throughout p-type conduction. If the contrary holds true, the magnitudes of the parameters ($|\varepsilon_0|$ and $|\gamma|$) are correct but the values themselves have reversed sings ($\varepsilon_0 \rightarrow -\varepsilon_0$, $\gamma \rightarrow -\gamma$).

5.1 Mechanically controlled break junctions

To start with, I will consider two single-molecule mechanically controlled break junctions fabricated with tolane anchored on gold electrodes using thiol and cyano groups (4,4′-bisthiotolane (BTT)) and 4,4′-biscyanotolane (BCT), respectively.[60] Digitized I–V curves for these junctions from ref. 60 are depicted by brown points in Fig. 3b and d.

Due to the substantial noise of the experimental (digitized) curves (brown points in Fig. 3a and c), data smoothing (red curves in Fig. 3a and c) represents the first step needed in reliably extracting the bias values V_{p+} and V_{p-} at the peaks of the curve for $|V|^{5/3}/|I|$.

Given the fact that the I–V curve for the symmetric BTT molecule is practically symmetric, the maxima are located
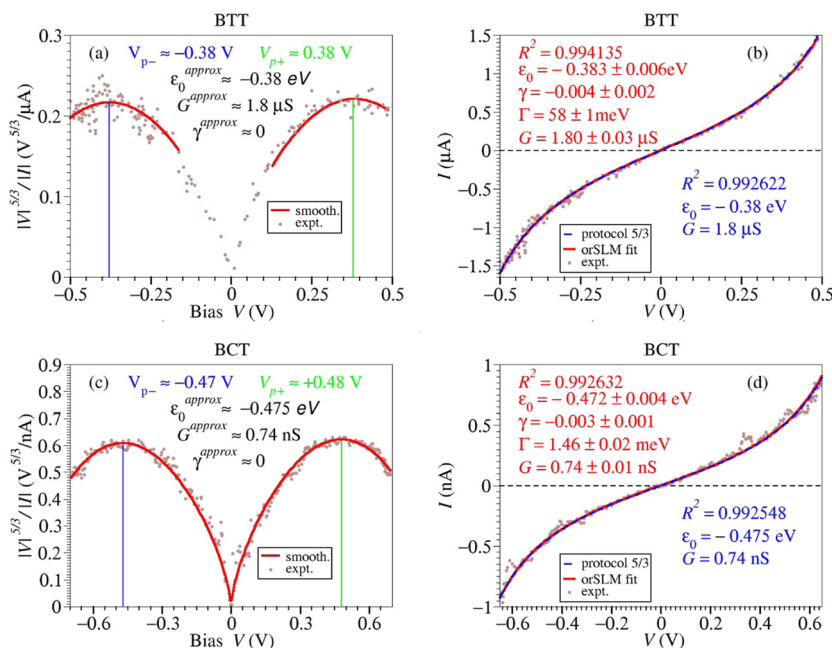

Fig. 3 Application of the five-thirds protocol to mechanically controlled break junctions fabricated with (4,4′-bisthiotolane (BTT)) (panels a and b) and 4,4′-biscyanotolane (BCT) (panels c and d). The experimental I–V data (brown points) were obtained by digitizing experimental I–V curves reported in ref. 60. Smoothing of the experimental data (brown points) yielded the (red) curves in panels a and c, which allow the reliable extraction of the biases V_{p+} and V_{p-} at the peaks of the $|V|^{5/3}/|I|$ curves. The values V_{p+} and V_{p-} and the corresponding currents $I_{p+} \equiv I(V_{p+})$ and $I_{p-} \equiv I(V_{p-})$ deduced from the I–V curves (panel b and d) serve as input in eqn (9). The results thus obtained (I–V curves and parameter values depicted in blue in panels b and d) have a quality comparable to those (depicted in red) deduced via data fitting to eqn (1) with adjustable parameters. The values of R^2 depicted in blue were computed via eqn (12).

8728 | *Phys. Chem. Chem. Phys.*, 2024, **26**, 8724–8733

This journal is © the Owner Societies 2024

symmetric around origin $V_{p+} \approx -V_{p-} \approx 0.38$ V. With the value $I_p = |I(V_{p\pm}| \approx 0.68$ nA) estimated from the experimental I–V curve (Fig. 3a) the conductance at low bias $G \approx 1.8$ nS can be deduced using eqn (11).

The I–V curve (brown points in Fig. 3d) for the asymmetric BCT molecule is slightly asymmetric. Accordingly, the peaks of the curve for $|V|^{5/3}/|I|$ are located slightly asymmetric around origin ($V_{p+} \approx 0.48$ V and $V_{p-} \approx -0.47$ V, *cf.* Fig. 3c). With these vales, the parameters ε_0, γ, and G of the BCT junction shown in the inset of Fig. 3c were estimated using eqn (9).

To illustrate the reliability of the five-thirds protocol for the BTT and BCT junctions considered, along the experimental I–V curve (brown points), I present both the fitting curve (line and parameter values pertaining to it in Fig. 3b and d are depicted in red) obtained using eqn (1) with adjustable model parameters and the I–V curve (line and parameter values pertaining to it in Fig. 3b and d are depicted in blue) computed *via* eqn (1) with the model parameters ε_0, γ, and G provided by the five-thirds protocol. As visible, the (blue) curves based on the five-thirds protocol and the fitting (red) curves cannot be distinguished from each other within the drawing accuracy. To put this excellent agreement in more quantitative terms, along with the coefficient of determination R^2 obtained by data fitting to eqn (1) (values written in red in Fig. 3b and d), I also present the counterparts of R^2 for the five-thirds protocol (values written in blue in Fig. 3b and d). The latter was obtained in the standard manner

$$R^2 = 1 - SS_{res}/SS_{tot} \qquad (12a)$$

$$SS_{res} = \sum_{k=1}^{n} \left[I_k^{exp} - I\left(V_k; \varepsilon_0^{approx}, \gamma^{approx}, G^{approx}\right)\right]^2 \qquad (12b)$$

$$SS_{tot} = \sum_{k=1}^{n} \left(I_k^{exp} - \bar{I}\right)^2; \ \bar{I} = \frac{1}{n}\sum_{k=1}^{n} I_k^{exp} \qquad (12c)$$

with n experimental values of the current I_k^{exp} and the values $I(V_k; \varepsilon_0^{approx}, \gamma^{approx}, G^{approx})$ computed from eqn (1) at the biases V_k sampled in experiment using the values ε_0^{approx}, γ^{approx}, G^{approx} of eqn (9).

5.2 STM break junctions

Next I will examine two single-molecule STM-BJ junctions with gold electrodes fabricated using 4,4′-diaminostilbene[61] (Fig. 4a–c) and phenyldithiol[62] (Fig. 4d and e).

In both cases no data smoothing was required to reliably extract V_{p+} and V_{p-} from the peaks of Fig. 4a and d. With these values and the pertaining currents I_{p+} and I_{p-} deduced from the experimental I–V curves of Fig. 4b and e (brown points), I arrived *via* eqn (9) at the blue I–V curves. Again, these curves excellently agree with the red I–V curves obtained by data fitting to eqn (1) with model parameters adequately adjusted.

The junction of 4,4′-diaminostilbene allows one to reveal the potential advantage of the present five-thirds protocol over the standard TVS-orSLM approach[12,14,15] based on the transition voltage V_t. As visible in Fig. 4c, the range of negative biases sampled in experiment[61] was not sufficiently broad. This prevents the determination of the model parameters using eqn (2).
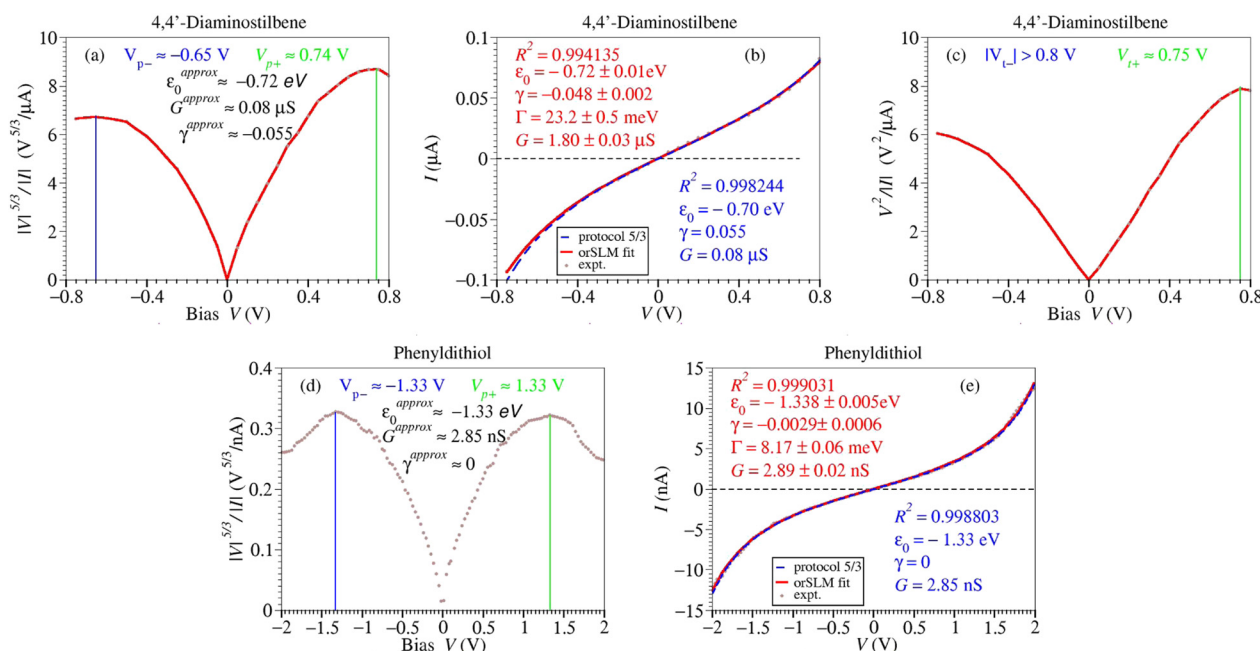

Fig. 4 Application of the five-thirds protocol to STM break junctions fabricated with 4,4′-diaminostilbene[61] (panels a, b, and c) and phenyldithiol (panel d and e).[62] The values V_{p+} and V_{p-} at the peaks of the $|V|^{5/3}/|I|$ curves and the corresponding currents $I_{p+} \equiv I(V_{p+})$ and $I_{p-} \equiv I(V_{p-})$ deduced from the I–V curves (panel b and e) serve as input in eqn (9). The results thus obtained (I–V curves and parameter values depicted in blue in panels b and e) have a quality comparable to those (depicted in red) deduced *via* data fitting to eqn (1) with adjustable parameters. The values of R^2 depicted in blue were computed *via* eqn (12). Panel c illustrates that the present five-thirds protocol can be also be applied in situations where the bias range sampled in experiment is too narrow for applying TVS.[14,15,50]

This journal is © the Owner Societies 2024

Phys. Chem. Chem. Phys., 2024, **26**, 8724–8733 | **8729**

That is, the five-thirds protocol can also be applied in cases where the use of eqn (2) is impractical.

5.3 CP-AFM molecular junctions

Smoothing the experimental transport data is also superfluous in analyzing the CP-AFM junctions of $1,1'$-,$4'$,$1''$-terphenyl-4-thiol and gold electrodes[63] (Fig. 5a and b) and of triphenyl-dithiol and silver electrodes (Fig. 5c and d).[64] Data smoothing is necessary to process the experimental I–V curve measured for the recently investigated CP-AFM junctions fabricated with 1-dodecyne (C12A) and silver electrodes anchored *via* alkynyl groups depicted in Fig. 5e and f.[65]

Inspection of the parameter values in the legends reveals that the five-thirds protocol works for all these cases.

5.4 Large-area molecular junctions

Last but not least, I will focus on three large area molecular junctions completely different from each other (Fig. 6).

The results depicted in Fig. 6a–c refer to a peptide-based junction fabricated with gold substrate and EGaIn top electrodes.[66] The specific peptide considered (G6W = GGGGGGW) consists of six glycines (G) with one aromatic amino acid at the C-terminus (tryptophan, W). Fig. 6d and e pertain to a junction consisting of a self-assembled monolayer of aryl octane (ArC8) with graphene contacts as protecting interlayer. The results depicted in Fig. 6f and g are for metal-free ITO-TCPP/PEDOT:PSS molecular junctions.[67] They were fabricated using carboxylic acid-modified porphyrin (*meso*-tetra(4-carboxyphenyl)porphyrin, TCPP) adsorbed to a bottom

electrode of indium tin oxide (ITO) and having the conductive PEDOT:PSS (poly(3,4-ethylenedioxythiophene):poly(styrenesul-fonate)) polymer as top electrode.[67] Recall that ITO is a degenerate n-type semiconductor possessing a wide band gap which makes it a transparent conductive electrode routinely employed in optoelectronic devices.

The message conveyed by the numerical values of the parameters inserted in Fig. 6 should be obvious. As in the preceding cases, they validate the five-thirds protocol also for the large-area junctions considered. To avoid some misunderstandings persisting in the literature, validation of the five-thirds protocol implicitly validates the orSLM for large area molecular tunnel junctions, the model on which this protocol relies. In addition, Fig. 6c reveals the same advantage of the five-thirds protocol over the conventional TVS approach based on eqn (2) already noted in the discussion related to Fig. 4c: to be applicable, the five-thirds protocol requires a narrower bias range than needed for TVS.

6 Additional remarks

For completeness, let me finally mention that, similar to eqn (9), lowest expansions in the location asymmetry (δV_κ) of the peaks $V_{\kappa+} = V_\kappa + \delta V_\kappa$ and $V_{\kappa-} = -V_\kappa + \delta V_\kappa$ of the general quantity $|V|^\kappa/|I|$ can also be deduced

$$|\varepsilon_0| \approx \sqrt{\frac{\kappa+1}{\kappa-1}\frac{eV_\kappa}{2}} \qquad (13a)$$
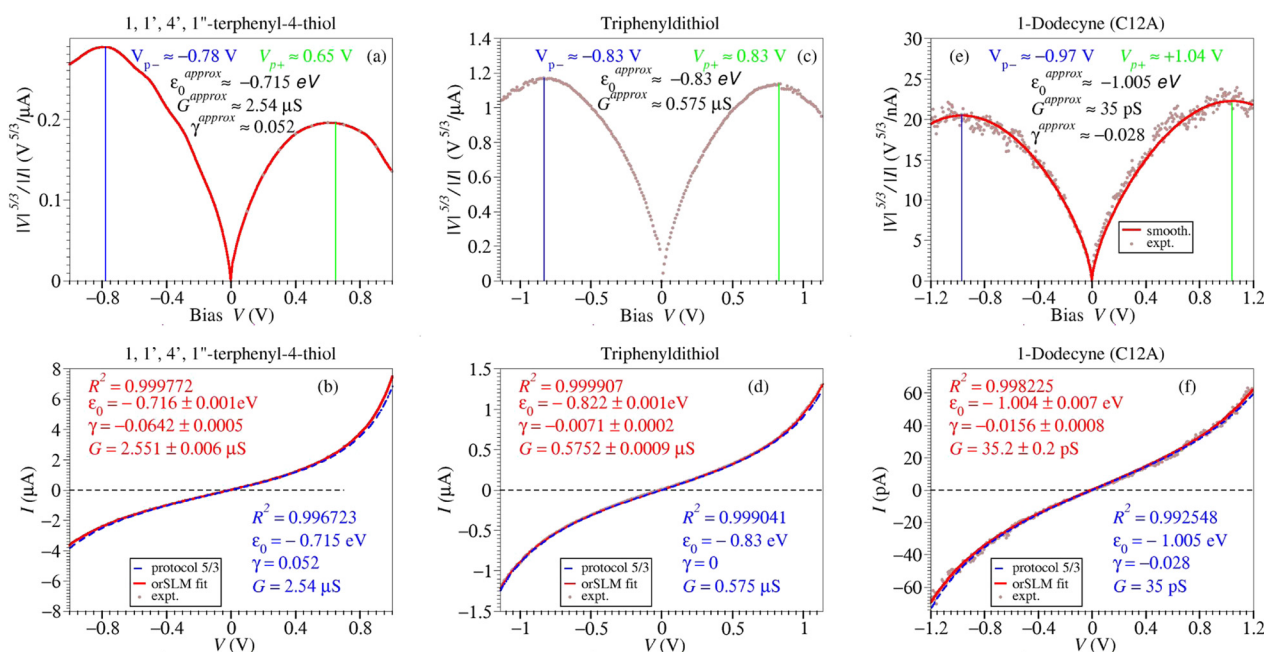

Fig. 5 Application of the five-thirds protocol to CP-AFM junctions fabricated with 1-,$1'$-,$4'$-,$1''$-terphenyl-4-thiol and gold electrodes (panels a and b),[63] with triphenyldithiol and silver electrodes (panels c and d),[64] and with 1-dodecyne and silver electrodes (panel e and f).[65] The values V_{p+} and V_{p-} at the peaks of the $|V|^{5/3}/|I|$ curves and the corresponding currents $I_{p+} \equiv I(V_{p+})$ and $I_{p-} \equiv I(V_{p-})$ deduced from the I–V curves (panel b and e) serve as input in eqn (9). The results thus obtained (I–V curves and parameter values depicted in blue in panels b and e) have a quality comparable to those (depicted in red) deduced *via* data fitting to eqn (1) with adjustable parameters. The values of R^2 depicted in blue were computed *via* eqn (12). The experimental data of panels d (junctions based on triphenyldithiols) and f (junctions based on 1-dodecyne (C12A)) were measured in conjunction with work reported in ref. 64 and 65 (courtesy of Zuoti Xie).
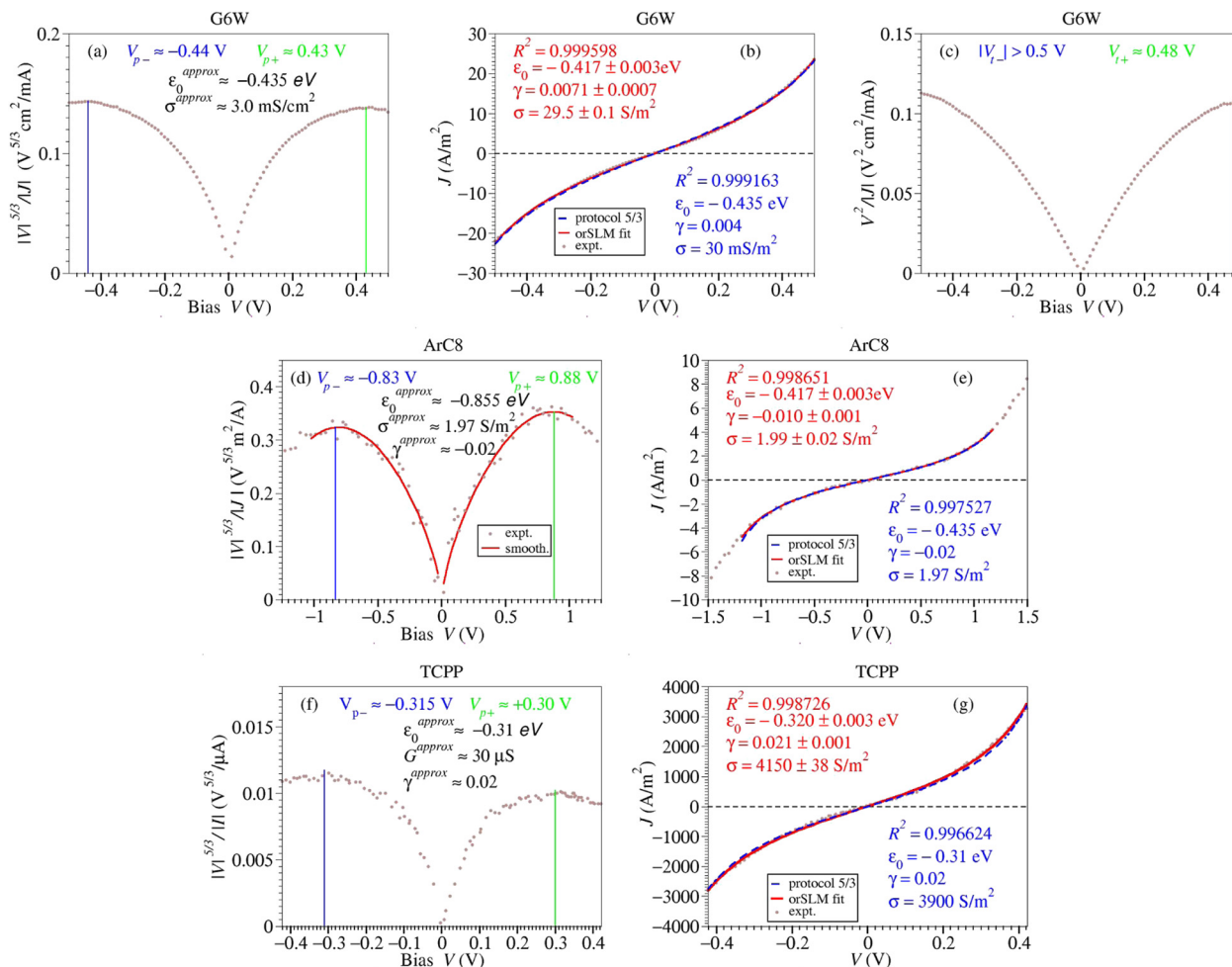
8730 | *Phys. Chem. Chem. Phys.*, 2024, **26**, 8724–8733

This journal is © the Owner Societies 2024

Fig. 6 Application of the five-thirds protocol to large area molecular junctions fabricated with a peptide (G6W)[66] (panels a, b, and c; experimental data: courtesy of Cunlan Guo), aryl octane (ArC8)[49] (panel d and e; experimental data from digitized Fig. 4a of ref. 49), and metal free ITO-based TCPP (panels f and g; experimental from digitized Fig. 4c of ref. 67). The values V_{p+} and V_{p-} at the peaks of the $|V|^{5/3}/|I|$ curves and the corresponding currents $I_{p+} \equiv I(V_{p+})$ and $I_{p-} \equiv I(V_{p-})$ deduced from the $I-V$ curves (panel b, e and g) serve as input in eqn (9). The results thus obtained ($I-V$ curves and parameter values depicted in blue in panels b, e and g) have a quality comparable to those (depicted in red) deduced via data fitting to eqn (1) with adjustable parameters. The values of R^2 depicted in blue were computed from eqn (12). Panel c illustrates that the present five-thirds protocol can be also be applied in situations where the bias range sampled in experiment is too narrow for applying TVS.[14,15,50] Because the transport measurements for large area junctions report current densities (J) rather than current intensities (I), values of the conductivity σ rather that conductance G are presented in this figure. In analyzing the ArC8[49] and TCPP[67] data, the bias range considered has been restricted to the bias range for which the orSLM applies.[10–12]

$$\gamma \approx \frac{\sqrt{\kappa^2-1}}{2\kappa} \frac{\delta V_\kappa}{V_\kappa} \text{sign} \varepsilon_0 \qquad (13b)$$

$$G \approx \frac{1}{\kappa+1}\left(\frac{I_{\kappa+}}{V_{\kappa+}}+\frac{I_{\kappa-}}{V_{\kappa+}}\right) \qquad (13c)$$

In the particular case $\kappa = 2$ ("transition voltage spectroscopy", TVS), they read

$$V_{t\pm} \equiv \pm V_t + \delta V_t, \; V_t = \frac{V_{t+}-V_{t-}}{2}, \; \delta V_t = \frac{V_{t+}+V_{t-}}{2}$$

$$|\varepsilon_0| \approx |\varepsilon_0^{approx}| = e\frac{\sqrt{3}}{2}V_t = e\frac{\sqrt{3}}{2}\frac{V_{t+}+|V_{t-}|}{2} \qquad (14a)$$

$$\gamma \approx \gamma^{approx} = \frac{\sqrt{3}}{4}\frac{\delta V_t}{V_t}\text{sign}\varepsilon_0$$
$$= \frac{\sqrt{3}}{2}\frac{V_{t+}-|V_{t-}|}{V_{t+}+|V_{t-}|}\text{sign}\varepsilon_0 \qquad (14b)$$

$$G \approx G^{approx} = \frac{1}{3}\left(\frac{I_{t+}}{V_{t+}}+\frac{I_{t+}}{V_{t+}}\right) \qquad (14c)$$

and represent a simpler alternative to eqn (2) in cases of typical $I-V$ asymmetries (reasonably small γ), as often the case in experiment.[14,15]

This journal is © the Owner Societies 2024

Phys. Chem. Chem. Phys., 2024, **26**, 8724–8733 | **8731**

7 Conclusion

By deducing eqn (9), in this paper I aimed at providing experimentalists with an extremely simple recipe ("five-thirds protocol") that allows straightforward extraction of the microscopic parameters of molecular tunnel junctions obviating I–V data fitting. As anticipated by the title, a pocket calculator is all what one needs for the few arithmetic operations to be performed in applying eqn (9).

By validating the "five-thirds protocol" for the platforms most commonly used to fabricate molecular tunnel junctions, I aimed at convincing the molecular electronics community on the generality of this approach enabling to gain important insight into the molecular structure–tunneling transport relationship. As seen, it can be applied even in situations beyond the reach of the (by now) standard TVS-based approach[12] whose broad usefulness has already be recognized.[13]

Conflicts of interest

There are no conflicts to declare.

Acknowledgements

References

1 S. Sze and K. K. Ng, *p–n Junctions*, John Wiley & Sons, Ltd, 2006, pp. 77–133.

2 M. T. Thompson, in *Intuitive Analog Circuit Design (Second Edition)*, ed. M. T. Thompson, Newnes, Boston, 2nd edn, 2014, pp. 53–86.

3 W. Shockley, *Bell Syst. Tech. J.*, 1949, **28**, 435–489.

4 W. Shockley, *Electrons and holes in semiconductors: with applications to transistor electronics*, Van Nostrand New York, New York, 1950.

5 C.-T. Sah, R. N. Noyce and W. Shockley, *Proc. IRE*, 1957, **45**, 1228–1243.

6 J. Moll, *Proc. IRE*, 1958, **46**, 1076–1082.

7 D. M. Newns, *Phys. Rev.*, 1969, **178**, 1123–1135.

8 P. W. Anderson, *Phys. Rev.*, 1961, **124**, 41–53.

9 W. Schmickler, *J. Electroanal. Chem.*, 1986, **204**, 31–43.

10 I. Bâldea, *Phys. Chem. Chem. Phys.*, 2023, **25**, 19750–19763.

11 I. Bâldea, *Phys. Chem. Chem. Phys.*, 2024, **26**, 6540–6556, DOI: 10.1039/D3CP05046G.

12 I. Bâldea, *Phys. Rev. B: Condens. Matter Mater. Phys.*, 2012, **85**, 035442.

13 D. Taherinia and C. D. Frisbie, *Phys. Chem. Chem. Phys.*, 2023, **25**, 32305–32316.

14 Z. Xie, I. Bâldea and C. D. Frisbie, *J. Am. Chem. Soc.*, 2019, **141**, 3670–3681.

15 Z. Xie, I. Bâldea and C. D. Frisbie, *J. Am. Chem. Soc.*, 2019, **141**, 18182–18192.

16 Q. V. Nguyen, Z. Xie and C. D. Frisbie, *J. Phys. Chem. C*, 2021, **125**, 4292–4298.

17 K. Smaali, N. Clément, G. Patriarche and D. Vuillaume, *ACS Nano*, 2012, **6**, 4639–4647.

18 T. K. Tran, K. Smaali, M. Hardouin, Q. Bricaud, M. Oçafrain, P. Blanchard, S. Lenfant, S. Godey, J. Roncali and D. Vuillaume, *Adv. Mater.*, 2013, **25**, 427–431.

19 D. Fracasso, M. I. Muglali, M. Rohwerder, A. Terfort and R. C. Chiechi, *J. Phys. Chem. C*, 2013, **117**, 11367–11376.

20 S. Guo, G. Zhou and N. Tao, *Nano Lett.*, 2013, **13**, 4326–4332.

21 K. Wu, M. Bai, S. Sanvito and S. Hou, *J. Chem. Phys.*, 2013, **139**, 194703.

22 W.-Y. Lo, L. Bi, L. Li, I. H. Jung and L. Yu, *Nano Lett.*, 2015, **15**, 958–962.

23 A. Xiang, M. Wang, H. Wang, H. Sun, S. Hou and J. Liao, *Chem. Phys.*, 2016, **465–466**, 40–45.

24 D. Nose, K. Dote, T. Sato, M. Yamamoto, H. Ishii and Y. Noguchi, *J. Phys. Chem. C*, 2015, **119**, 12765–12771.

25 A. Kovalchuk, T. Abu-Husein, D. Fracasso, D. Egger, E. Zojer, M. Zharnikov, A. Terfort and R. Chiechi, *Chem. Sci.*, 2015, **7**, 781–787.

26 C. Jia, A. Migliore, N. Xin, S. Huang, J. Wang, Q. Yang, S. Wang, H. Chen, D. Wang, B. Feng, Z. Liu, G. Zhang, D.-H. Qu, H. Tian, M. A. Ratner, H. Q. Xu, A. Nitzan and X. Guo, *Science*, 2016, **352**, 1443–1445.

27 D. Xiang, X. Wang, C. Jia, T. Lee and X. Guo, *Chem. Rev.*, 2016, **116**, 4318–4440.

28 Q. Wang, R. Liu, D. Xiang, M. Sun, Z. Zhao, L. Sun, T. Mei, P. Wu, H. Liu, X. Guo, Z.-L. Li and T. Lee, *ACS Nano*, 2016, **10**, 9695–9702.

29 H. Jeong, Y. Jang, D. Kim, W.-T. Hwang, J.-W. Kim and T. Lee, *J. Phys. Chem. C*, 2016, **120**, 3564–3572.

30 L. Li, W.-Y. Lo, Z. Cai, N. Zhang and L. Yu, *Chem. Sci.*, 2016, **7**, 3137–3141.

31 Z. Cai, W.-Y. Lo, T. Zheng, L. Li, N. Zhang, Y. Hu and L. Yu, *J. Am. Chem. Soc.*, 2016, 10630–10635.

32 W.-Y. Lo, N. Zhang, Z. Cai, L. Li and L. Yu, *Acc. Chem. Res.*, 2016, **49**, 1852–1863.

33 X. Yi, N. V. Izarova, M. Stuckart, D. Guérin, L. Thomas, S. Lenfant, D. Vuillaume, J. van Leusen, T. Duchoň, S. Nemšák, S. D. M. Bourone, S. Schmitz and P. Kögerler, *J. Am. Chem. Soc.*, 2017, **139**, 14501–14510.

34 Z. Cai, N. Zhang, M. A. Awais, A. S. Filatov and L. Yu, *Angew. Chem., Int. Ed.*, 2018, **57**, 6442–6448.

35 I. Jeong and H. Song, *Appl. Spectrosc. Rev.*, 2018, **53**, 246–263.

36 S. Valianti, J.-C. Cuevas and S. S. Skourtis, *J. Phys. Chem. C*, 2019, **123**, 5907–5922.

37 M.-W. Gu, H. H. Peng, I.-W. P. Chen and C.-H. Chen, *Nat. Mater.*, 2021, **20**, 658–664.

38 Y. Liu, X. Qiu, S. Soni and R. C. Chiechi, *Chem. Phys. Rev.*, 2021, **2**, 021303.

39 Y. Kim, K. Im and H. Song, *Materials*, 2022, **15**, 774.

40 M. Carlotti, S. Soni, A. Kovalchuk, S. Kumar, S. Hofmann and R. C. Chiechi, *ACS Phys. Chem. Au*, 2022, **2**, 179–190.

8732 | *Phys. Chem. Chem. Phys.*, 2024, **26**, 8724–8733

This journal is © the Owner Societies 2024

41 J. Jang, P. He and H. J. Yoon, *Acc. Chem. Res.*, 2023, **56**, 1613–1622.

42 I. Bâldea, *Phys. Chem. Chem. Phys.*, 2024, **26**, 7230–7235, DOI: **10.1039/D2CP05110A**.

43 W. Schmickler and N. Tao, *Electrochim. Acta*, 1997, **42**, 2809–2815.

44 W. Han, E. N. Durantini, T. A. Moore, A. L. Moore, D. Gust, P. Rez, G. Leatherman, G. R. Seely, N. Tao and S. M. Lindsay, *J. Phys. Chem. B*, 1997, **101**, 10719–10725.

45 W. Wang, T. Lee and M. A. Reed, *Phys. Rev. B: Condens. Matter Mater. Phys.*, 2003, **68**, 035416.

46 I. V. Pobelov, Z. Li and T. Wandlowski, *J. Am. Chem. Soc.*, 2008, **130**, 16045–16054.

47 A. R. Garrigues, L. Yuan, L. Wang, E. R. Mucciolo, D. Thompon, E. del Barco and C. A. Nijhuis, *Sci. Rep.*, 2016, **6**, 26517.

48 V. Delmas, V. Diez-Cabanes, C. van Dyck, E. Scheer, K. Costuas and J. Cornil, *Phys. Chem. Chem. Phys.*, 2020, **22**, 26702–26706.

49 K. Im, D.-H. Seo and H. Song, *Crystals*, 2022, **12**, 767.

50 J. M. Beebe, B. Kim, J. W. Gadzuk, C. D. Frisbie and J. G. Kushmerick, *Phys. Rev. Lett.*, 2006, **97**, 026801.

51 I. Bâldea, *Phys. Chem. Chem. Phys.*, 2015, **17**, 15756–15763.

52 I. Bâldea, Z. Xie and C. D. Frisbie, *Nanoscale*, 2015, **7**, 10465–10471.

53 I. Bâldea, *Europhys. Lett.*, 2012, **98**, 17010.

54 R. M. Metzger, *Chem. Rev.*, 2015, **115**, 5056–5115.

55 M. S. Johnson, L. D. Wickramasinghe, C. N. Verani and R. M. Metzger, *J. Phys. Chem. C*, 2016, **120**, 10578–10583.

56 Z. Xie, I. Bâldea, Q. Nguyen and C. D. Frisbie, *Nanoscale*, 2021, **13**, 16755–16768.

57 R. P. Sullivan, J. T. Morningstar, E. Castellanos-Trejo, M. E. Welker and O. D. Jurchescu, *Nano Lett.*, 2023, **23**, 10864–10870.

58 R. Metzger, *Nanoscale*, 2018, **10**, 10316–10332.

59 R. Gupta, J. A. Fereiro, A. Bayat, A. Pritam, M. Zharnikov and P. C. Mondal, *Nat. Rev. Chem.*, 2023, **7**, 106–122.

60 L. A. Zotti, T. Kirchner, J.-C. Cuevas, F. Pauly, T. Huhn, E. Scheer and A. Erbe, *Small*, 2010, **6**, 1529–1535.

61 J. R. Widawsky, M. Kamenetska, J. Klare, C. Nuckolls, M. L. Steigerwald, M. S. Hybertsen and L. Venkataraman, *Nanotechnology*, 2009, **20**, 434009.

62 W. Lee and P. Reddy, *Nanotechnology*, 2011, **22**, 485703.

63 A. Tan, S. Sadat and P. Reddy, *Appl. Phys. Lett.*, 2010, **96**, 013110.

64 Z. Xie, I. Bâldea, C. Smith, Y. Wu and C. D. Frisbie, *ACS Nano*, 2015, **9**, 8022–8036.

65 Y. Chen, I. Bâldea, Y. Yu, Z. Liang, M.-D. Li, E. Koren and Z. Xie, *Langmuir*, 2024, DOI: **10.1021/acs.langmuir.3c03759**.

66 L. Su, Y. Zhang, Q. Pan, H. Liang, H. Wang and C. Guo, *New J. Chem.*, 2023, **47**, 17277–17283.

67 S. Sergani, Y. Furmansky and I. Visoly-Fisher, *Nanotechnology*, 2013, **24**, 455204.

This journal is © the Owner Societies 2024

Phys. Chem. Chem. Phys., 2024, **26**, 8724–8733 | **8733**